

Exchange-based CNOT gates for singlet-triplet qubits with spin orbit interaction

Jelena Klinovaja,¹ Dimitrije Stepanenko,¹ Bertrand I. Halperin,² and Daniel Loss¹

¹*Department of Physics, University of Basel, Klingelbergstrasse 82, CH-4056 Basel, Switzerland*

²*Department of Physics, Harvard University, 17 Oxford St., 5 Cambridge, MA 02138, USA*

(Dated: March 8, 2013)

We propose a scheme for implementing the CNOT gate over qubits encoded in a pair of electron spins in a double quantum dot. The scheme is based on exchange and spin orbit interactions and on local gradients in Zeeman fields. We find that the optimal device geometry for this implementation involves effective magnetic fields that are parallel to the symmetry axis of the spin orbit interaction. We show that the switching times for the CNOT gate can be as fast as a few nanoseconds for realistic parameter values in GaAs semiconductors. Guided by recent advances in surface codes, we also consider the perpendicular geometry. In this case, leakage errors due to spin orbit interaction occur but can be suppressed in strong magnetic fields.

PACS numbers: 73.21.La; 73.63.Kv; 85.35.Be

I. INTRODUCTION

Standard quantum computing [1] is based on encoding, manipulating, and measuring quantum information encoded in the state of a collection of quantum two-level systems - qubits. Spin-1/2 is an ideal implementation of a qubit, since it is a natural two-level system, and every pure state of a spin-1/2 corresponds to a state of a qubit. For this reason, spins have been considered as carriers of quantum information in a variety of proposals [2]. The initial proposal [3] called for spins in single-electron quantum dots electrically manipulated by the exchange interaction and local time-dependent Zeeman fields. A variety of other encoding schemes and manipulation techniques [4–11] rely upon encoded qubits. In these schemes, the simplicity of qubit states and minimal number of physical carriers of quantum information are traded for less stringent requirements for experimental implementations. On one hand, the alternative setups protect from the most common types of errors by decoupling the computational degrees of freedom from the most common sources of noise, and therefore allow for longer gating times. On the other hand, in some alternative setups the manipulation without fast switching of the local magnetic fields becomes possible.

The optimization in the encoding and manipulation protocols is always guided by the state of the art in the experiments. Recent results suggest that spin qubits can reside in a variety of material hosts with novel properties. Quantum dots in graphene [12] and carbon nanotubes [13] are less susceptible to the decoherence due to nuclei and spin-orbit interaction. Spins in nanowires show very strong confinement in two spatial directions, and the gating is comparably simple [8, 9]. In hole systems, the carriers have distinct symmetry properties, and show coupling to the nuclear spins of a novel kind [14]. Recently, the experiments in silicon [15] have demonstrated coherent manipulation of spins similar to the one achieved in the GaAs-based nanostructures. Within these hosts, the manipulation techniques that use exchange interaction, spatially inhomogeneous time independent Zeeman split-

ting, and nuclear hyperfine interactions are within reach. Despite these developments, GaAs remains a promising route to spin qubits due to the highly advanced experimental techniques developed for this material.

Here, we study the implementation of the quantum gates on the encoded two-spin singlet-triplet (ST) qubits [4, 5, 7, 10, 16, 17] using resources that closely resemble the ones available in the current experimental setups. There, the application of the time-dependent electric fields through the gates fabricated into a structure [11] are preferred to time-dependent local magnetic fields. In addition, the nuclear spins [7, 16–19] and inhomogeneous magnetic fields [20, 21] are possible resources for spin control. In the setups based on semiconductors, the electrons or holes in the quantum dots are influenced by the spin orbit interaction (SOI), which can contribute to the control [22].

In this work we present a scheme for control of ST-qubits which uses switching of the exchange interaction as a primary resource. We consider the scheme that is optimized for the application of quantum gates in the network of quantum dots. The construction of the CNOT gate uses pulses of the exchange interaction as the only parameter that is time dependent. The exchange interaction itself is not sufficient for the universal quantum computation over the ST-qubits due to its high symmetry. The additional symmetry breaking is provided by nonuniform, but static magnetic fields. These fields describe the influence both of magnetic fields, provided by the nearby magnets, and of the coupling to the nuclear spins in the host material via hyperfine interaction. Depending on the scheme used for the application of the quantum gates, the optimal geometry is either the one in which the magnetic fields point parallel to the axis of symmetry of the SOI or perpendicular to it.

One major problem in the realization of two-qubit quantum gates (in particular, we consider here the CNOT gate based on conditional phase gates), is the possibility of leakage errors where the spin states defining the logical qubit leave the computational space. These errors move the state of four spins from the 4-dimensional com-

putational space of two qubits into some other portion of the 16-dimensional Hilbert space of four spin-1/2 particles. We consider two ways of addressing this problem. One scheme possesses the axial symmetry due to the fact that the SOI vector and magnetic fields are parallel. For this ‘parallel scheme’ we are able to construct a perfect CNOT gate, if we are able to control all the available parameters. Having in mind 2D architectures, we also consider the CNOT gate between two qubits in the case when the SOI vector and magnetic fields are perpendicular to each other. Here we cannot prevent the leakage out of the computational space, however, we show that it is suppressed by a ratio between the SOI and Zeeman energy coming from a strong external magnetic field.

All our constructions assume that the controlled interactions are switched in time by rectangular pulses. Any deviations from this form of time dependence lead to additional corrections and affect the fidelity of the gate.

The paper is organized as follows. In Sec. II, we introduce the model for the double dots and effective Hamiltonians for field gradients and exchange and spin orbit interactions. In Sec. III, we consider the parallel geometry and derive the CNOT gate via the conditional phase gates and swap gates, all based on exchange. There we also give estimates for the switching times. The scheme for the perpendicular geometry is then addressed in Sec. IV, and we conclude in Sec. V.

II. THE EFFECTIVE MODEL

We consider in the following singlet-triplet (ST) qubits that are implemented by two electrons confined to a double quantum dot system [4, 5], see Figs. 1 and 2. Such ST-qubits have been realized successfully in several labs [23], and single and two-qubit operations have also been

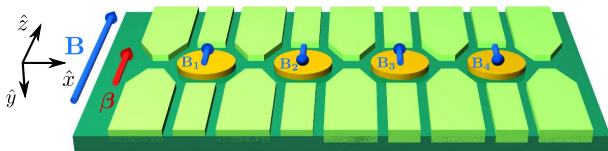


FIG. 1: Parallel geometry: four quantum dots (yellow discs) aligned along the x-axis in the presence of an external magnetic field \mathbf{B} that is applied parallel to the SOI vector β (red arrow), which must be perpendicular to the line of the dots and which we take to be the z-direction. At each dot, there is a local magnetic field \mathbf{B}_i (blue arrows), also assumed to be parallel to \mathbf{B} , but with alternating orientations as indicated. The direction of \mathbf{B} defines the spin quantization axis. The dots are defined electrostatically by metallic gates (light green structures). Each dot contains a spin-1/2, and the exchange (J_{ij}) and the SOI-induced (β_{ij}) interactions between the spins can be controlled by changing the electrostatic potential between the dots. The dots 1 and 2 (from left to right) define the first ST-qubit, and the dots 3 and 4 the second ST-qubit.

demonstrated recently [7, 10, 17, 24]. There are several schemes for the fundamental CNOT gate, which can be divided into two classes, schemes which make use of exchange interaction and schemes which do not, but instead rely on coupling of dipole moments [10]. The latter schemes has the disadvantage to be rather slow and also to be affected by charge noise rather strongly. Here, we focus on exchange-based schemes specifically adapted to quantum dots in III-V semiconducting materials, that have the SOI, such as in GaAs or InAs quantum dots. Although the SOI is typically small compared to the level spacing of the dots, it needs to be taken into account in order to achieve high fidelities in gate operations.

We focus now on two such ST-qubits and assume them to be encoded in four quantum dots that are arranged in a row, see Figs. 1 and 2. The external magnetic field \mathbf{B} is assumed to give the largest energy scale and determines the spin quantization axis z . The Hilbert space of four spins-1/2 is spanned by $2^4 = 16$ basis states. The total spin of the system is given by $\hat{\mathbf{S}} = \sum_{i=1}^4 \hat{\mathbf{S}}_i$, where $\hat{\mathbf{S}}_i$ is a spin-1/2 operator acting on the spin in a dot $i = 1, 2, 3, 4$. Due to axial symmetry, the z-component, \hat{S}^z , becomes a good quantum number, and the eigenstates corresponding to $S^z = 0$ span a six-dimensional subspace. We define the computational basis of the two ST-qubits in this subspace as

$$\begin{aligned} |00\rangle &= |\downarrow\uparrow\downarrow\uparrow\rangle, & |11\rangle &= |\uparrow\downarrow\uparrow\downarrow\rangle, \\ |01\rangle &= |\downarrow\uparrow\uparrow\downarrow\rangle, & |10\rangle &= |\uparrow\downarrow\downarrow\uparrow\rangle, \end{aligned} \quad (1)$$

where $\{0,1\}^{\otimes 2}$ denotes the ST-qubit space, ‘ \uparrow ’ and ‘ \downarrow ’ denote states of the quantum dot spins corresponding to the projection $S_i^z = \pm 1/2$ on the z axis. The remaining two states,

$$|l_1\rangle = |\uparrow\uparrow\downarrow\downarrow\rangle, \quad |l_2\rangle = |\downarrow\downarrow\uparrow\uparrow\rangle, \quad (2)$$

belong to the non-computational leakage space.

Besides the externally applied magnetic field \mathbf{B} , we allow also for local magnetic fields \mathbf{B}_i that are constant in time (at least over the switching time of the gate). Such local fields can be generated e.g. by nearby micromagnets [21] or by the hyperfine field [25–30] produced by the nuclear spins of the host material. In the latter case, in order to reach a high fidelity, it is important to perform a nuclear state narrowing [25], *i.e.* to suppress the natural variance $\delta B_i \sim A/\sqrt{N} \sim 10\text{mT}$ to a smaller value. In the ideal case, one should try to reach a limit where $|\mathbf{B}_i| \sim 50\text{mT} \ll |\mathbf{B}|$ and the fluctuations in \mathbf{B}_i are much smaller than $|\mathbf{B}_i|$.

The magnetic fields \mathbf{B}_i are assumed to point along the external field \mathbf{B} , so that they preserve the axial symmetry of the problem. However, the \mathbf{B}_i ’s should have different values (to create field gradients between the dots), a simple scenario being local fields of opposite directions on neighboring dots, see Figs. 1 and 2. The corresponding Zeeman Hamiltonian is given by

$$H^B = \sum_{i=1}^4 (b + b_i) \hat{S}_i^z, \quad (3)$$

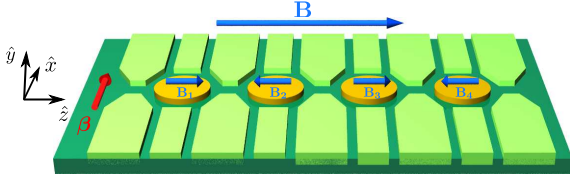


FIG. 2: Perpendicular geometry: similar to the setup shown in Fig. 1 but with the difference that here the SOI vector β (red arrow) is *perpendicular* to the magnetic fields \mathbf{B} and \mathbf{B}_i , which define the spin quantization axis z .

where the effective magnetic fields are defined in terms of energy as $b = g\mu_B B$ and $b_i = g\mu_B B_i$, respectively, with g being the electron g -factor and μ_B the Bohr magneton.

The exchange interaction $J_{ij}(t)$ couples the electron spins of nearest neighbor dots i and j and can be controlled electrostatically [7, 21, 23]. If the tunnel barrier between the dots is high we can treat them as independent. If the tunnel barrier is lowered and/or a detuning between the dots is applied, the two spins interact with each other, leading to an effective description in terms of an Heisenberg Hamiltonian [3, 22, 31],

$$H^{ex} = J_{12}(t)\hat{\mathbf{S}}_1 \cdot \hat{\mathbf{S}}_2 + J_{23}(t)\hat{\mathbf{S}}_2 \cdot \hat{\mathbf{S}}_3 + J_{34}(t)\hat{\mathbf{S}}_3 \cdot \hat{\mathbf{S}}_4. \quad (4)$$

We assume that the magnetic field is sufficiently large compared to exchange energies, *i.e.* $J_{ij} \ll B$, to avoid admixture of triplets via the SOI (see the discussion of perpendicular geometry below).

We note that ideally it is best to switch the exchange J_{ij} by changing the corresponding inter-dot barrier-height or distance, instead of detuning the double dot by a bias ϵ . Detuning is harmful for two reasons. First, detuning can admix other unwanted states (for example, (0,2)S, see Fig. 2 in [22]). To analyze the errors coming from detuning, one needs to go beyond the effective spin Hamiltonian and consider the microscopic model for the double dots which includes Rashba and Dresselhaus SOI and inhomogeneous fields, see Ref. [22]. Second, the control of J_{ij} via the tunnel barrier preserves the symmetry of the charge distribution in the double dot and thus, in particular, avoids the creation of dipole moments. In contrast, such dipole moments are unavoidable for detuning, and in the regime with $dJ_{ij}/d\epsilon \neq 0$ charge noise can enter most efficiently the qubit space, causing gate errors and decoherence of the ST-qubits [25]. Thus, symmetric exchange switching is expected to be more favourable for achieving high gate fidelities.

Next, we account for the effects of spin orbit interaction. Following Refs. [32–34] we model the SOI by a Dzyaloshinskii-Moriya (DM) term for two neighboring quantum dots (see e.g. Eq. (1) in [33]),

$$H_{ij}^{SOI} = \beta_{ij}(t) \cdot (\hat{\mathbf{S}}_i \times \hat{\mathbf{S}}_j), \quad (5)$$

where the SOI vector $\beta_{ij}(t)$ is perpendicular to the line connecting the dots. First we consider a ‘parallel geometry’ (see Fig. 1) where the SOI vectors β_{ij} are all parallel

to each other and the magnetic fields \mathbf{B} and \mathbf{B}_i are assumed to be parallel to the SOI vectors. This preserves the axial symmetry of the spin system, and by definition, we choose the direction of \mathbf{B} to be the z -axis. This leads to

$$H_{\parallel}^{SOI} = \sum_{i,j} \beta_{ij}(t) (\hat{S}_i^x \hat{S}_j^y - \hat{S}_i^y \hat{S}_j^x), \quad (6)$$

where the summation runs over neighboring dots i and j . The strength of the SOI, β_{ij} , depends on the distance between the dots as well as on the tunnel coupling between them. This allows us to assume that both $J_{ij}(t)$ and $\beta_{ij}(t)$ are switched on and off simultaneously [35–37].

We note here that both H^{ex} and H_{\parallel}^{SOI} , being axially symmetric interactions, preserve the z -component of the total spin S^z . This means that our set-up is protected from leakage to the subspace with $S^z \neq 0$. However, it is not protected from the leakage to the non-computational space given by Eq. (2). By a proper design of gates this leakage can be minimized.

Alternatively, in a ‘perpendicular geometry’ (see Fig. 2) the axis of the quantum dots is aligned parallel to the applied magnetic field, in the z -direction. The SOI vector β_{ij} is perpendicular to this, and we take it to be in x -direction. The corresponding Hamiltonian becomes

$$H_{\perp}^{SOI} = \sum_{i,j} \beta_{ij}(t) (\hat{S}_i^y \hat{S}_j^z - \hat{S}_i^z \hat{S}_j^y). \quad (7)$$

Here, the SOI vector β_{ij} breaks the axial symmetry of the system, and the total spin S^z is no longer a good quantum number. As a consequence, leakage into the non-computational space $S^z \neq 0$ is possible, in principle. However, this coupling involves higher-energy states and can thus be suppressed by choosing a sufficiently large magnetic field such that $\beta/B \ll 1$. In contrast, the SOI does not couple states within the computational space, since the matrix elements of H_{\perp}^{SOI} between the states $|\downarrow\uparrow\rangle$ and $|\uparrow\downarrow\rangle$ vanish.

III. PARALLEL GEOMETRY

In this section we concentrate on the parallel geometry, see Fig. 1. Using the axial symmetry of the problem we are able to construct a sequence of gate operations that implements the CNOT gate [1], defined on the logical ST-qubits given in Eq. (1) by $U_{CNOT}|a,b\rangle = |a, a \oplus b\rangle$, where $a, b = 0, 1$.

One important step in this construction is the implementation of the $\pi/4$ -gate $U_{\pi/4}$ (see discussion below and [1]). For this gate we propose the following scheme consisting of four steps,

$$C_{23} \rightarrow (\pi_{12}, \pi_{34}) \rightarrow C_{23} \rightarrow (\pi_{12}, \pi_{34}), \quad (8)$$

where the conditional phase gate C_{23} exchange-couples the dots 2 and 3 and adds a phase factor to the two ST-qubits (see below). The swap gates π_{12} and π_{34} exchange

spin states on the dots 1 and 2 and the dots 3 and 4, and can be performed in parallel.

A major issue in the implementation of $U_{\pi/4}$ is the avoidance of leakage errors during the coupling of qubits. To keep qubits in the computational space, operations on spins 2 and 3 must be constructed in such a way that the resulting gate is diagonal in the basis given by Eq. (1). This can be achieved in two ways. The first approach is to use strong pulses that lead to fast rotations around the Bloch sphere. The second approach is to use adiabatic pulses that are protected from the leakage to states with different energies [38]. However, the adiabaticity requires a longer pulse time. In the present work we focus on the first approach.

A. Conditional phase gate C_{23}

In this subsection we describe the phase gate, C_{23} , involving the exchange and SOI interactions only between dot 2 and 3, while dots 1 and 4 are decoupled from dots 2 and 3, *i.e.*, $J_{12} = J_{34} = 0$ and $\beta_{12} = \beta_{34} = 0$. In this case, the effective Hamiltonian is given by

$$H^C = H^B + H^{ex} + H_{\parallel}^{SOI} = H_1^C + H_{23}^C + H_4^C, \quad (9)$$

where we present it in block-diagonal form. The part of the Hamiltonian $H_i^C = (b + b_i)\hat{S}_i^z$ acts only on spins located at the dot $i = 1, 4$. The other part of the Hamiltonian, H_{23}^C , acts on spins located at the dots 2 and 3,

$$H_{23}^C = (b + b_2)\hat{S}_2^z + (b + b_3)\hat{S}_3^z + J_{23}\hat{\mathbf{S}}_2 \cdot \hat{\mathbf{S}}_3 + \beta_{23}(\hat{S}_2^x \hat{S}_3^y - \hat{S}_2^y \hat{S}_3^x). \quad (10)$$

Here, we assume a rectangular pulse shape for the exchange and spin orbit interactions, and from now on we treat J_{23} and β_{23} as time-independent parameters. In this case, the unitary gate U^C is a simple exponential of the Hamiltonian,

$$U^C = e^{-iH^C T_C} = e^{-iH_1^C T_C} e^{-iH_{23}^C T_C} e^{-iH_4^C T_C}. \quad (11)$$

The spins of dot 1 and 4 do not change in time apart from a phase factor coming from the corresponding magnetic field. In contrast, the spins of dot 2 and 3 change in time and acquire phases, as we describe next. For this we express H_{23}^C as matrix in the basis $\{|\uparrow\uparrow\rangle, |\uparrow\downarrow\rangle, |\downarrow\uparrow\rangle, |\downarrow\downarrow\rangle\}$,

$$\begin{pmatrix} H_+^C & 0 & 0 \\ 0 & H_0^C & 0 \\ 0 & 0 & H_-^C \end{pmatrix}, \quad (12)$$

where the block-diagonal form reflects the conservation of S^z . In the case of two parallel spins, the corresponding Hamiltonian is given by $H_{\pm}^C = J_{23}/4 \pm (b_2 + b_3)/2$, which just assigns a phase to the spins. In the case of antiparallel spins, the Hamiltonian H_0^C is given by

$$H_0^C = \frac{1}{2} \begin{pmatrix} -J_{23}/2 + \Delta b_{23} & J_{23} + i\beta_{23} \\ J_{23} - i\beta_{23} & -J_{23}/2 - \Delta b_{23} \end{pmatrix}, \quad (13)$$

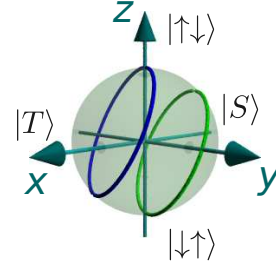


FIG. 3: The Bloch sphere is defined with the north pole corresponding to $|\uparrow\downarrow\rangle$ and the south pole corresponding to $|\downarrow\uparrow\rangle$. The effect of the unitary evolution operator U_0^C [see Eq. (17)] on a state in the space $\{|\uparrow\downarrow\rangle, |\downarrow\uparrow\rangle\}$ is equivalent to the rotation on the Bloch sphere around the vector $J_{23}\mathbf{e}_x - \beta_{23}\mathbf{e}_y + \Delta b_{23}\mathbf{e}_z$. The conditional phase gate C_{23} corresponds to the full rotation on the Bloch sphere (shown by blue and green circles).

where $\Delta b_{23} = b_2 - b_3$. Here, H_0^C describes the coupling between the states $|\uparrow\downarrow\rangle$ and $|\downarrow\uparrow\rangle$, which, in general, leads to leakage errors. This leakage can be prevented by choosing the pulse duration, T_C , in such a way that the corresponding unitary operator $U_0^C = \exp[-iH_0^C T_C]$ is diagonal in the basis $\{|\uparrow\downarrow\rangle, |\downarrow\uparrow\rangle\}$. It is more convenient to consider the evolution given by H_0^C on the Bloch sphere. For that we rewrite H_0^C in terms of pseudospins,

$$H_0^C = -J_{23}/4 + (\tilde{J}_{23}/2) \mathbf{n}_{23} \cdot \boldsymbol{\tau}, \quad (14)$$

$$\tilde{J}_{23} = \sqrt{J_{23}^2 + \beta_{23}^2 + (\Delta b_{23})^2}, \quad (15)$$

$$\mathbf{n}_{23} = (J_{23}, -\beta_{23}, \Delta b_{23})/\tilde{J}_{23}, \quad (16)$$

where the unit vector \mathbf{n}_{23} defines the rotation axis on the Bloch sphere, see Fig. 3, and the pseudospin, acting on the states $\{|\uparrow\downarrow\rangle, |\downarrow\uparrow\rangle\}$, is described by the Pauli matrices $\boldsymbol{\tau}$. The north pole corresponds to $|\uparrow\downarrow\rangle$ and the south pole to $|\downarrow\uparrow\rangle$. The exchange interaction, J_{23} , being the largest scale in H_0^C , forces \mathbf{n}_{23} to be aligned mostly along the x -axis. If we neglect the SOI and any field gradients, the rotation on the Bloch sphere takes place in the yz -plane. In the presence of SOI and field gradients the rotation axis \mathbf{n}_{23} deviates from the x -axis.

The unitary time evolution operator U_0^C corresponding to H_0^C takes the form

$$U_0^C = \exp(i\alpha_C/2)(\cos \alpha_C + i \mathbf{n}_{23} \cdot \boldsymbol{\tau} \sin \alpha_C), \quad (17)$$

where $\alpha_C = \tilde{J}_{23} T_C/2$. The duration of a pulse is determined by the condition that we obtain full rotations on the Bloch sphere (see Fig. 3),

$$T_C = \frac{2\pi N_C}{\tilde{J}_{23}}, \quad (18)$$

where N_C is a positive integer. Note that deviations from Eq. (18) lead, again, to leakage errors.

As a result, the qubit states with parallel spins on dot

2 and 3, acquire the phases

$$\begin{aligned}\phi_{01} &= \frac{1}{2}(J_{23}/2 - b_1 + b_2 + b_3 - b_4)T_C, \\ \phi_{10} &= \frac{1}{2}(J_{23}/2 + b_1 - b_2 - b_3 + b_4)T_C,\end{aligned}\quad (19)$$

while the qubit states with antiparallel spins on dot 2 and 3 acquire the phases

$$\begin{aligned}\phi_{11} &= \frac{1}{2}(b_1 - b_4 - (-1)^{N_C} J_{23}/2)T_C, \\ \phi_{00} &= \frac{1}{2}(-b_1 + b_4 - (-1)^{N_C} J_{23}/2)T_C.\end{aligned}\quad (20)$$

Here, ϕ_{ab} corresponds to a phase acquired by a two-qubit state $|ab\rangle$. We note that phases produced by the magnetic fields terms will be canceled during the second C_{23} pulse after the π -pulses have been applied to the qubits.

B. Swap gates π_{12} and π_{34}

In this subsection we discuss the swap gates π_{12} and π_{34} that exchange spin states between dot 1 and 2, and dot 3 and 4, respectively. The swap operation is a one-qubit-operation, so dots 2 and 3 should be decoupled during the swap pulse, *i.e.*, $J_{23} = 0$ and $\beta_{23} = 0$. The swap gate $\pi = (\pi_{12}, \pi_{34})$ is implemented, again, by a rectangular pulse and all parameters are assumed to stay constant during the switching process. This simplifies the unitary evolution operator,

$$U^\pi = U_{12}^\pi U_{34}^\pi = e^{-iH_{12}^\pi T_\pi} e^{-iH_{34}^\pi T_\pi}. \quad (21)$$

Further, we focus on the first ST-qubit (dots 1 and 2) and consider only π_{12} (π_{34} can be obtained analogously). We also note that since S^z is conserved, the final state is always given by a linear combination of the states $|\downarrow\uparrow\rangle$ and $|\uparrow\downarrow\rangle$ on dot 1 and 2. Within this subspace the effective Hamiltonian is given by

$$H_{12}^\pi = \frac{1}{2} \begin{pmatrix} -J_{12}/2 + \Delta b_{12} & J_{12} + i\beta_{12} \\ J_{12} - i\beta_{12} & -J_{12}/2 - \Delta b_{12} \end{pmatrix}, \quad (22)$$

or in pseudospin representation [see Eq. (14)],

$$H_{12}^\pi = -J_{12}/4 + (\tilde{J}_{12}/2) \mathbf{n}_{12} \cdot \boldsymbol{\tau}, \quad (23)$$

$$\tilde{J}_{12} = \sqrt{J_{12}^2 + \beta_{12}^2 + (\Delta b_{12})^2}, \quad (24)$$

$$\mathbf{n}_{12} = (J_{12}, -\beta_{12}, \Delta b_{12})/\tilde{J}_{12}, \quad (25)$$

where $\Delta b_{12} = b_1 - b_2$ and the Pauli matrix τ_i acts in the pseudospin space spanned by $|\uparrow\downarrow\rangle$ and $|\downarrow\uparrow\rangle$. Again, the unit vector \mathbf{n}_{12} defines the rotation axis. The corresponding unitary evolution operator reduces to the form

$$U_{12}^\pi = \exp(i\alpha_\pi/2)(\cos \alpha_\pi + i\mathbf{n}_{12} \cdot \boldsymbol{\tau} \sin \alpha_\pi), \quad (26)$$

where $\alpha_\pi = \tilde{J}_{12}T_\pi/2$.

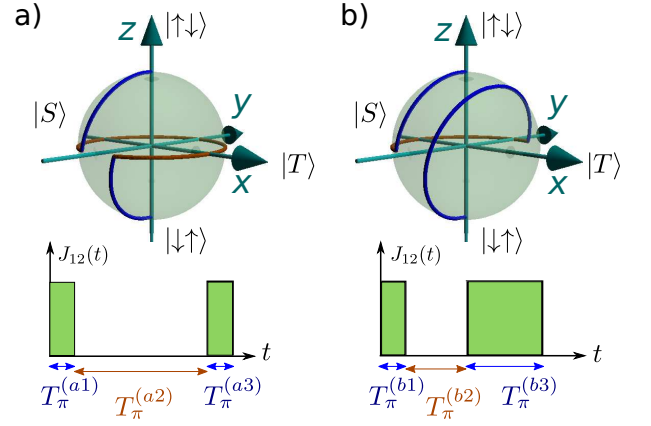


FIG. 4: Two schemes for the swap gate, $\pi_{12}: |\uparrow\downarrow\rangle \rightarrow |\downarrow\uparrow\rangle$, composed of three consecutive rotations on the Bloch sphere where the offset induced by Δb_{12} and β_{12} is fully compensated. a) First, starting from the north pole, we turn on J_{12} and β_{12} to induce rotation around $J_{12}\mathbf{e}_x - \beta_{12}\mathbf{e}_y + \Delta b_{12}\mathbf{e}_z$ (upper blue arc) until we reach the equator where we turn off J_{12} and β_{12} . Second, we let the state precess around the z -axis in the equatorial plane until the mirror point of the starting point on the equator is reached (brown arc). Third, we induce once more rotation around $J_{12}\mathbf{e}_x - \beta_{12}\mathbf{e}_y + \Delta b_{12}\mathbf{e}_z$ (lower blue arc) until we reach the south pole. Lower panel: associated rectangular gate pulses and switching times $T_\pi^{(a1,a2,a3)}$ for the three steps. b) Alternative scheme where during the second step the state precesses along the equator until it reaches the point diametrically opposite to its starting point (brown arc).

The swap operation should exchange the states $|\uparrow\downarrow\rangle$ and $|\downarrow\uparrow\rangle$. In the absence of SOI and field gradients, the unitary evolution operator U_{12}^π corresponds to a rotation around the x -axis ($\mathbf{n}_{12} = \mathbf{e}_x$) in the yz -plane. At half the period, $T_\pi^0 = \pi/2\tilde{J}_{12}$, a state evolves from the north to the south pole and vice versa, *i.e.*, $U_{12}^\pi|T_\pi^0\rangle \propto \tau_x$.

However, in the presence of SOI and/or field gradients, the rotation axis \mathbf{n}_{12} is not aligned with \mathbf{e}_x (compare with Fig. 3), so the trajectory starting at the north (south) pole would never go exactly through the south (north) pole. The corresponding deviations lead to errors in the π_{12} gate on the order of $\sqrt{\Delta b_{12}^2 + \beta_{12}^2}/J_{12}$. This means that it is impossible to produce a perfect swap operation with only one single rectangular pulse. However, by applying a sequence of several rectangular pulses, it is still possible to produce a perfect π_{12} gate, as we demonstrate next.

Indeed, this goal can be achieved by the following three steps (see also Fig. 4). First, we switch on the exchange interaction J_{12} between the dots 1 and 2 (this also automatically switches on the SOI β_{12}). We assume J_{12} to be larger than Δb_{12} and/or β_{12} . The rotation axis \mathbf{n}_{12} in polar coordinates is given by

$$\mathbf{n}_{12} = (\sin \vartheta \cos \varphi, \sin \vartheta \sin \varphi, \cos \vartheta). \quad (27)$$

From now on we work in the coordinate system in which the x -axis points along $J_{12}\mathbf{e}_x - \beta_{12}\mathbf{e}_y$, so $\varphi = 0$ and

$0 \leq \cos \vartheta = \Delta b_{12}/\tilde{J}_{12} \leq 1/\sqrt{2}$. The strength and the duration of the rectangular pulse is chosen in such a way that the rotation reaches the equator of the Bloch sphere. The initial and final vectors on the Bloch sphere are given by

$$\phi_i = (0, 0, 1), \quad (28)$$

$$\phi_f = (\cot \vartheta, \sqrt{\sin(2\vartheta - \pi/2)}/\sin \vartheta, 0), \quad (29)$$

allowing us to find the rotation angle $\alpha_\pi^{(a1)} = \pi/2 + \arcsin(\cot^2 \vartheta)$, and the corresponding pulse duration

$$T_\pi^{(a1)} = [\pi + 2 \arcsin(\cot^2 \vartheta)]/2\tilde{J}_{12}. \quad (30)$$

Second, after switching off exchange and spin orbit interactions, $J_{12} = 0$ and $\beta_{12} = 0$, the rotation takes place around the z -axis in the equatorial plane, at a precession frequency determined by the field gradient Δb_{12} . The rotation angle becomes $\alpha_\pi^{(a2)} = 2[\pi - \arccos(\cot \vartheta)]$, and the pulse duration is given by

$$T_\pi^{(a2)} = \alpha_\pi^{(a2)}/\Delta b_{12}. \quad (31)$$

Finally, we repeat the first step by applying a pulse of the same strength J_{12} (β_{12}) and during the same time, $T_\pi^{(a3)} = T_\pi^{(a1)}$.

An alternative scheme (b) is presented in Fig. 4b. During the second step the state evolves on the Bloch sphere only over half of the equator, $\alpha_\pi^{(b2)} = \pi$, with the corresponding pulse duration $T_\pi^{(b2)} = \alpha_\pi^{(b2)}/\Delta b_{12}$. The

duration of the third pulse is given by

$$T_\pi^{(b3)} = [3\pi - 2 \arcsin(\cot^2 \vartheta)]/2\tilde{J}_{12}. \quad (32)$$

The second step is the slowest one in these schemes, so the scheme (b) has an advantage over the scheme (a) by being faster as it requires less rotation on the equator. However, scheme (b) requires better control of parameters, since $T_\pi^{(b1)} \neq T_\pi^{(b3)}$.

Here we note that it is also possible to switch off the exchange coupling J_{12} not only on the equator but also at any other point on the Bloch sphere. Moving away from the equator speeds up the gate performance, but demands greater precision in the tuning, since the rotation proceeds along a smaller arc and in shorter time.

The scheme presented above confirms that it is possible to construct a perfect π swap gate even in the presence of z -component of the SOI vector, β_{12} , or local field gradients, $\Delta \mathbf{b}_{12}$, by adjusting the pulse durations. The other two components of the SOI vector couple states of different total spin S^z , and thus cause leakage errors. Therefore, it is optimal to orient the magnetic fields (defining the spin quantization axis z) along the SOI vector, β_{12} .

C. CNOT gate

After the execution of the four-step sequence given by Eq. (8) an initial qubit state is restored but with a phase factor [see Eqs. (19) and (20)]:

$$\begin{aligned} [00] &\xrightarrow{C_{23}} e^{i\phi_{00}} [00] \xrightarrow{(\pi_{12}, \pi_{34})} e^{i\phi_{00}} [11] \xrightarrow{C_{23}} e^{i(\phi_{11}+\phi_{00})} [11] \xrightarrow{(\pi_{12}, \pi_{34})} [00] e^{i(\phi_{11}+\phi_{00})}, \\ [11] &\xrightarrow{C_{23}} e^{i\phi_{11}} [11] \xrightarrow{(\pi_{12}, \pi_{34})} e^{i\phi_{11}} [00] \xrightarrow{C_{23}} e^{i(\phi_{11}+\phi_{00})} [00] \xrightarrow{(\pi_{12}, \pi_{34})} [11] e^{i(\phi_{11}+\phi_{00})}, \\ [01] &\xrightarrow{C_{23}} e^{i\phi_{01}} [01] \xrightarrow{(\pi_{12}, \pi_{34})} e^{i\phi_{01}} [11] \xrightarrow{C_{23}} e^{i(\phi_{01}+\phi_{10})} [11] \xrightarrow{(\pi_{12}, \pi_{34})} [00] e^{i(\phi_{01}+\phi_{10})}, \\ [10] &\xrightarrow{C_{23}} e^{i\phi_{10}} [10] \xrightarrow{(\pi_{12}, \pi_{34})} e^{i\phi_{10}} [01] \xrightarrow{C_{23}} e^{i(\phi_{01}+\phi_{10})} [01] \xrightarrow{(\pi_{12}, \pi_{34})} [10] e^{i(\phi_{01}+\phi_{10})}, \end{aligned} \quad (33)$$

with $\phi_{01} + \phi_{10} = -(\phi_{11} + \phi_{00}) = J_{23}T_C/2$, where we assume N_C [see Eq. (18)] to be even. The total gate acting on the qubits as defined by Eq. (33) can be written in the compact form

$$e^{-i(J_{23}T_C/2)\sigma_1^z\sigma_2^z}, \quad (34)$$

where the Pauli matrix σ_1^j acts on the first ST-qubit (formed by dot 1 and 2) and σ_2^j on the second one (formed by dot 3 and 4) with $j = x, y, z$. Choosing

$$T_C = \left(4\pi m - \frac{\pi}{2}\right)/J_{23}, \quad (35)$$

where m is a positive integer, we obtain the $\pi/4$ -gate,

$$U_{\pi/4} = e^{i\frac{\pi}{4}\sigma_1^z\sigma_2^z}. \quad (36)$$

Both Eqs. (18) and (35) should be satisfied simultaneously. For example, if $m = 1$ and $N_C = 2$, we get

$$T_C = \frac{\pi}{2} \sqrt{\frac{15}{\Delta b_{23}^2 + \beta_{23}^2}}, \quad (37)$$

$$J_{23} = \frac{7}{\sqrt{15}} \sqrt{\Delta b_{23}^2 + \beta_{23}^2}. \quad (38)$$

From this we can estimate the total switching time to perform the $\pi/4$ -gate that is a sum of the switching times at each step [see Eq. (8)]. For the scheme discussed in Subsecs. III A and III B the slowest part is given by the swap gates π_{12} and π_{34} , whose switching time is limited by field gradients (due to nuclear spins [7, 16–19] and/or micromagnets [20, 21]), $|\Delta b_{12}| = |\Delta b_{34}| \approx 10$ mT, which corresponds to $T_\pi^{(b2)} \approx 10$ ns. The gate can be faster

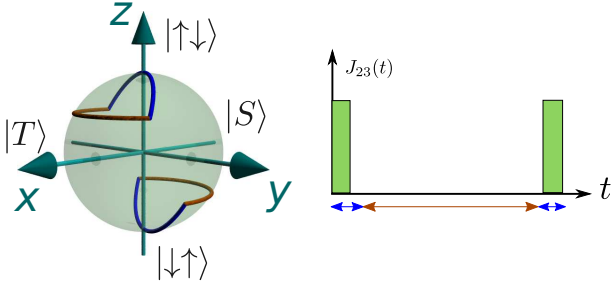


FIG. 5: An alternative scheme for the conditional phase gate C_{23} (see also Fig. 3). Instead of the rotation with the pulse defined by Eqs. (18) and (35) we consider a sequence of three pulses. During the first and the third pulses (blue arcs) the state precesses quickly acquiring the $\pi/4$ -phase, see Eq. (35). During the second pulse, $J_{23} = 0$, the state precesses around the z -axis over a shorter path than the one in Fig. 3. As a result, the switching is faster.

if the rotations around the z -axis are performed not on the equator but more closely to the poles. This allows us to decrease the switching time of the swap gate to 2 ns; however, this would require a more precise control over the pulses. The same trick can be used to decrease the switching time of the conditional phase gate C_{23} (compare Figs. 3 and 5). If field gradients larger than 10 mT are used, the switching rates will be proportionately larger.

Using the $\pi/4$ -gate, we construct the controlled phase flip (CPF) gate $U_{CPF} = \text{diag}(1, 1, 1, -1)$ (see footnote [13] in [3]) as

$$U_{CPF} = U_{\pi/4} e^{-i\frac{\pi}{4}(\sigma_1^z + \sigma_2^z - 1)}. \quad (39)$$

Finally, we obtain the CNOT gate,

$$U_{CNOT} = \begin{pmatrix} \mathbb{I} & 0 \\ 0 & \sigma_2^x \end{pmatrix}, \quad (40)$$

by using the CPF gate and performing a basis rotation on qubit 2 (a single-qubit rotation by $\pi/2$ about the y -axis),

$$U_{CNOT} = e^{i\frac{\pi}{4}\sigma_2^y} U_{CPF} e^{-i\frac{\pi}{4}\sigma_2^y}. \quad (41)$$

In summary, the full sequence of operations for the CNOT gate, U_{CNOT} , is given by

$$e^{i\frac{\pi}{4}\sigma_2^y} [(\pi_{12}\pi_{34})C_{23}(\pi_{12}\pi_{34})C_{23}] e^{-i\frac{\pi}{4}(\sigma_1^z + \sigma_2^z)} e^{-i\frac{\pi}{4}\sigma_2^y}. \quad (42)$$

We note again that this result has been derived under the assumption of rectangular pulse shapes. This is certainly an idealization, and in practice we expect deviations from this shape to cause errors for the gates and to affect the gate fidelity. The study of this issue, being very important for practical purposes, requires a separate investigation and is beyond the scope of this work.

IV. PERPENDICULAR GEOMETRY

In the previous section we have discussed the parallel geometry for which we were able to construct a perfect CNOT gate under the assumption that we have a complete control over the parameters. The CNOT gate, together with single-qubit gates, allows us to simulate any other quantum gate and its implementation is a crucial step toward the realization of a quantum computer [1]. In a next step, many such elementary gates need to be connected into a large network. In recent years, the surface code [39] has emerged as one of the most promising platforms for this goal due to its large threshold of about 1% for fault tolerant error correction [39]. This platform requires a two-dimensional (2D) geometry and can be implemented in semiconductors of the type considered here. [11].

The basic 2D scheme is illustrated in Fig. 6. There, we show an array of quantum dots where two neighboring dots in a given row represent one ST-qubit. These quantum dots are embedded in a semiconductor where the SOI is of the same type in the entire structure. As a typical example we mention Rashba and/or Dresselhaus SOI that both depend on the momentum of the electron. As a result, the direction of the SOI vector β is always perpendicular to the line along which two quantum dots are coupled by exchange interaction [22]. Thus, for the coupling of two such qubits in the *same* row, the SOI vector β is parallel to the external magnetic field \mathbf{B} , so we can use the scheme designed for the parallel geometry in the previous section. In contrast, if we want to couple two qubits from *neighboring* rows, we should also consider a ‘perpendicular geometry’ (see Figs. 1 and 6) in which the SOI vector β is perpendicular to the magnetic field \mathbf{B} .

This perpendicular geometry is characterized by several features. As was mentioned before, the axial symmetry in this case is broken by the SOI, leading to the coupling between computational ($S_z = 0$) and non-

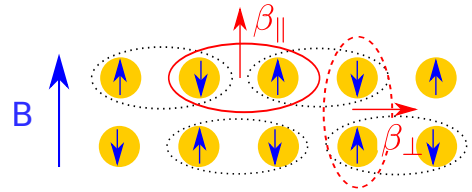


FIG. 6: Schematic setup for 2D architecture. Two dots define an ST-qubit (black dotted ellipses). An external magnetic field \mathbf{B} and local magnetic fields (blue arrows) are parallel. In the case of the coupling between two qubits from the same row (red solid ellipse) the SOI vector β_{\parallel} is parallel to the magnetic field \mathbf{B} , corresponding to the parallel geometry (see Fig. 1). In the case of coupling between two qubits from two neighboring rows (red dashed ellipse) the SOI vector β_{\perp} is perpendicular to the magnetic field \mathbf{B} , corresponding to the perpendicular geometry (see Fig. 2).

computational ($S_z \neq 0$) space. If the magnetic field B is sufficiently large to split the triplet levels T_{\pm} far away from the computational space ($g\mu_B B \gg \beta$), we can neglect this leakage. We estimate for GaAs $B = 5\text{T} \approx 100\mu\text{eV}/g\mu_B$. At the same time, the SOI does not couple states within the computational space, so for the realization of the phase gate C_{23} and the swaps gates π_{12} and π_{34} we can use the same scheme as in Sec. III only with $\beta = 0$.

V. CONCLUSIONS

We have studied the implementation of the CNOT gate for ST-qubits in a model that is appropriate for current experiments [7, 17, 24]. The setup consists of an array of quantum dots with controlled growth direction and the relative orientation of the dots. Pairs of neighboring dots build the ST-qubits, where the quantization axis is determined by an externally applied magnetic field \mathbf{B} . Moreover, we introduce an inhomogeneity in magnetic fields, \mathbf{B}_i , by local micromagnets or by the hyperfine field. The resources used for time-dependent control are the exchange interaction $J_{ij}(t)$, the field gradients $\Delta B_{ij}(t)$, and the SOI vector $\beta_{ij}(t)$.

If the SOI vector β is parallel to the external (\mathbf{B}) and local magnetic fields (\mathbf{B}_i), we are able to construct a perfect scheme for the CNOT gate based on the $\pi/4$ -phase gate, $U_{\pi/4}$, consisting of four basic steps. Two of the steps involve interaction of spins that belong to different

qubits, and open the possibility of leakage errors. Under condition of total control over system parameters, we show that the leakage can be eliminated. In the other two steps, the tuning of exchange interaction enables perfect swap gates even in the presence of field gradients and SOI.

Motivated by recent results on the surface code, we shortly comment also on the 2D architecture. Here we encounter a situation in which the SOI vector β and the magnetic fields, \mathbf{B} and \mathbf{B}_i , are perpendicular. In this case, the leakage to the non-computational space with $S_z \neq 0$ is inevitable. However, it can be made very small as long as $\beta/g\mu_B B \ll 1$.

Depending on the pulsing scheme, the switching times for the conditional phase gate are shown to lie in the range 1-100 ns for typical GaAs parameters. Compared to the experimentally established decoherence times of about 250 μs [17], this switching is sufficiently fast and shows that a CNOT gate based on exchange is a promising candidate for experimental realizations.

Acknowledgments

We acknowledge discussions with Andrew Doherty, Charles Marcus, Izhar Neder, and Mark Rudner. This work is supported by IARPA/MQCO program, DARPA/QUEST program, the Swiss NSF, NCCR Nanoscience, and NCCR QSIT.

-
- [1] A. Nielsen, Michael and I. L. Chuang, *Quantum Computation and Quantum Information* (Cambridge University Press, Cambridge, 2000).
 - [2] C. Kloeffer and D. Loss, arXiv:1204.5917 (2012).
 - [3] D. Loss and D. P. DiVincenzo, Phys. Rev. A **57**, 120 (1998).
 - [4] J. Levy, Phys. Rev. Lett. **89**, 147902 (2002).
 - [5] S. C. Benjamin, Phys. Rev. A **64**, 054303 (2001).
 - [6] D. P. DiVincenzo, D. Bacon, J. Kempe, G. Burkard, and K. B. Whaley, Nature **408**, 339 (2000).
 - [7] J. R. Petta, A. C. Johnson, J. M. Taylor, E. A. Laird, A. Yacoby, M. D. Lukin, C. M. Marcus, M. P. Hanson, and A. C. Gossard, Science **309**, 2180 (2005).
 - [8] M. Trif, V. N. Golovach, and D. Loss, Phys. Rev. B **75**, 085307 (2007).
 - [9] M. Trif, V. N. Golovach, and D. Loss, Phys. Rev. B **77**, 045434 (2008).
 - [10] M. D. Shulman, O. E. Dial, S. P. Harvey, H. Bluhm, V. Umansky, and A. Yacoby, Science **336**, 202 (2012).
 - [11] L. Trifunovic, O. Dial, M. Trif, J. R. Wootton, R. Abebe, A. Yacoby, and D. Loss, Phys. Rev. X **2**, 011006 (2012).
 - [12] B. Trauzettel, D. V. Bulaev, D. Loss, and G. Burkard, Nat. Phys. **3**, 192 (2007).
 - [13] D. V. Bulaev, B. Trauzettel, and D. Loss, Phys. Rev. B **77**, 235301 (2008).
 - [14] J. Fischer, W. A. Coish, D. V. Bulaev, and D. Loss, Phys. Rev. B **78**, 155329 (2008).
 - [15] B. M. Maune, M. G. Borselli, B. Huang, T. D. Ladd, P. W. Deelman, K. S. Holabird, A. A. Kiselev, I. Alvarado-Rodriguez, R. S. Ross, A. E. Schmitz, et al., Nature **481**, 344 (2012).
 - [16] A. C. Johnson, J. R. Petta, C. M. Marcus, M. P. Hanson, and A. C. Gossard, Phys. Rev. B **72**, 165308 (2005).
 - [17] H. Bluhm, S. Foletti, I. Neder, M. Rudner, D. Mahalu, V. Umansky, and A. Yacoby, Nat. Phys. **7**, 109 (2011).
 - [18] S. Tarucha, Y. Kitamura, T. Kodera, and K. Ono, physica status solidi (b) **243**, 3673 (2006).
 - [19] H. Ribeiro, J. R. Petta, and G. Burkard, Phys. Rev. B **82**, 115445 (2010).
 - [20] J. Baugh, Y. Kitamura, K. Ono, and S. Tarucha, Phys. Rev. Lett. **99**, 096804 (2007).
 - [21] R. Brunner, Y.-S. Shin, T. Obata, M. Pioro-Ladrière, T. Kubo, K. Yoshida, T. Taniyama, Y. Tokura, and S. Tarucha, Phys. Rev. Lett. **107**, 146801 (2011).
 - [22] D. Stepanenko, M. Rudner, B. I. Halperin, and D. Loss, Phys. Rev. B **85**, 075416 (2012).
 - [23] R. Hanson, L. P. Kouwenhoven, J. R. Petta, S. Tarucha, and L. M. K. Vandersypen, Rev. Mod. Phys. **79**, 1217 (2007).
 - [24] C. Barthel, J. Medford, C. M. Marcus, M. P. Hanson, and A. C. Gossard, Phys. Rev. Lett. **105**, 266808 (2010).
 - [25] W. A. Coish and D. Loss, Phys. Rev. B **70**, 195340 (2004).
 - [26] A. Khaetskii, D. Loss, and L. Glazman, Phys. Rev. B **67**,

- 195329 (2003).
- [27] I. A. Merkulov, A. L. Efros, and M. Rosen, Phys. Rev. B **65**, 205309 (2002).
 - [28] L. Cywiński, W. M. Witzel, and S. Das Sarma, Phys. Rev. B **79**, 245314 (2009).
 - [29] R.-B. Liu, W. Yao, and L. Sham, Advances in Physics **59**, 703 (2010).
 - [30] S. Foletti, H. Bluhm, D. Mahalu, V. Umansky, and A. Yacoby, Nat. Phys. **5**, 903 (2009).
 - [31] G. Burkard, D. Loss, and D. P. DiVincenzo, Phys. Rev. B **59**, 2070 (1999).
 - [32] N. E. Bonesteel, D. Stepanenko, and D. P. DiVincenzo, Phys. Rev. Lett. **87**, 207901 (2001).
 - [33] G. Burkard and D. Loss, Phys. Rev. Lett. **88**, 047903 (2002).
 - [34] D. Stepanenko, N. E. Bonesteel, D. P. DiVincenzo, G. Burkard, and D. Loss, Phys. Rev. B **68**, 115306 (2003).
 - [35] L. Shekhtman, O. Entin-Wohlman, and A. Aharony, Phys. Rev. Lett. **69**, 836 (1992).
 - [36] T. Yildirim, A. B. Harris, O. Entin-Wohlman, and A. Aharony, Phys. Rev. Lett. **73**, 2919 (1994).
 - [37] F. Baruffa, P. Stano, and J. Fabian, Phys. Rev. B **82**, 045311 (2010).
 - [38] A. Doherty *et al.*, to be published.
 - [39] D. S. Wang, A. G. Fowler, and L. C. L. Hollenberg, Phys. Rev. A **83**, 020302(R) (2011).